Oncogene (2011) 1–10

www.nature.com/onc

ORIGINAL ARTICLE

Identification of phosphorylase kinase as a novel therapeutic target through high-throughput screening for anti-angiogenesis compounds in zebrafish

S Camus[1], C Quevedo[2], S Menéndez[1], I Paramonov[1], PFW Stouten[3], RAJ Janssen[4], S Rueb[5], S He[5], BE Snaar-Jagalska[5], L Laricchia-Robbio[1] and JC Izpisua Belmonte[1,6]

[1]*Center for Regenerative Medicine in Barcelona, Barcelona, Spain;* [2]*Biobide SL, San Sebastián, Spain;* [3]*Galapagos, NV, Mechelen, Belgium;* [4]*Galapagos, BV, Leiden, The Netherlands;* [5]*Institute of Biology, Leiden University, Leiden, The Netherlands and* [6]*Salk Institute for Biological Studies, La Jolla, CA, USA*

Angiogenesis is essential for development and tumor progression. With the aim of identifying new compound inhibitors of the angiogenesis process, we used an established enhanced green fluorescent protein-transgenic zebrafish line to develop an automated assay that enables high-throughput screening of compound libraries in a whole-organism setting. Using this system, we have identified novel kinase inhibitor compounds that show anti-angiogenic properties in both zebrafish *in-vivo* system and in human endothelial cell *in-vitro* angiogenesis models. Furthermore, we have determined the kinase target of these compounds and have identified and validated a previously uncharacterized involvement of phosphorylase kinase subunit G1 (PhKG1) in angiogenesis *in vivo*. In addition, we have found that PhKG1 is upregulated in human tumor samples and that aberrations in gene copy number of PhK subunits are a common feature of human tumors. Our results provide a novel insight into the angiogenesis process, as well as identify new potential targets for anti-angiogenic therapies.
Oncogene advance online publication, 19 December 2011; doi:10.1038/onc.2011.594

Keywords: phosphorylase kinase; PhK; angiogenesis; zebrafish; cancer

Introduction

The formation of the first primitive vessels from mesoderm-derived angioblasts (endothelial precursor cells) occurs through the vasculogenesis process. Later growth of both physiological and pathological vessels occurs through angiogenesis, which is the process of growth of microvessels from existing vasculature (Eilken and Adams, 2010). Pathological angiogenesis is associated with tumor progression and is a pre-requisite of tumor growth and metastasis (Carmeliet and Jain, 2000). Therefore, inhibitors of angiogenesis are desirable candidates for anti-tumoral therapies, and angiogenic factors that diffuse from tumor cells to stimulate angiogenesis have been extensively investigated as therapeutic targets. A number of inhibitors of angiogenic factors are currently undergoing phase III clinical trials. Several such compounds are kinase inhibitors, suggesting that kinase inhibition represents a relevant and effective approach. Recently, a number of anti-angiogenic compounds have been approved by the US Food and Drug Administration for therapeutic use (Gragoudas *et al*., 2004; Hurwitz *et al*., 2004; Folkman, 2007).

Zebrafish provide a useful vertebrate model organism due to their high fecundity, short-generation times, and ease of housing and maintaining large numbers, which provides them with statistical power and adaptability to high-throughput systems that are impossible with mammalian models. Furthermore, there is a high degree of conservation between zebrafish and other species regarding the pathways involved in tumorigenesis (including many tumor suppressor pathways such as the p53 (Berghmans *et al*., 2005), phosphatase and tensin homolog (Faucherre *et al*., 2008), retinoblastoma protein (pRB) (Edmunds *et al*., 2002), lkb (Marshall *et al*., 2011), etc) and angiogenesis (Lyons *et al*., 1998; Liang *et al*., 2001). Zebrafish have therefore emerged as an effective model for cancer studies as well as a valuable screening tool as they offer the biological complexity of an *in vivo* system, whilst meeting the requirement for large numbers and efficient drug uptake from the water (Parng *et al*., 2002; Kidd and Weinstein, 2003). Furthermore, they present powerful imaging solutions through *in-vivo* fluorescent labeling of desired organs, such as the vasculature system. Several successful screens have been performed in zebrafish, including two screens directed at compound inhibitors of angiogenesis (Tran *et al*., 2007; Wang *et al*., 2010).

In this study, we have taken advantage of the *TG(Fli1:EGFP)* zebrafish line (Lawson and Weinstein, 2002), in which the vascular system is visible through endothelial-specific enhanced green fluorescent protein (EGFP) expression, to screen putative kinase inhibitors from the BioFocus SoftFocus library SFK33 (Galapagos, BV, Leiden, The Netherlands) to identify inhibitors of angiogenesis. We have developed an automated assay

Correspondence: Dr JC Izpisua Belmonte, Salk Institute for Biological Studies, 10010 N Torrey Pines Road, La Jolla, CA 92037, USA.
E-mail: belmonte@salk.edu
Received 8 September 2011; revised 29 October 2011; accepted 7 November 2011

to enable high-throughput compound screening and have identified anti-angiogenic compounds, two of which were further studied to elucidate the anti-angiogenic mechanism. Furthermore, we have identified phosphorylase kinase (PhK) as a target and verified its involvement in angiogenesis and value as a potential target for anti-tumoral therapeutics.

Results

In zebrafish, the process of angiogenesis drives the formation and sprouting of the intersegmental vessels (ISV) from the vasculogenic vessels of the dorsal aorta (DA) between 16–19 h post fertilization (hpf; Isogai *et al*., 2001). A labeled diagram outlining the vasculature of the *TG(Fli1:EGFP)* zebrafish line is provided in Supplementary Figure 1.

To discover new inhibitory compounds of the angiogenesis process, an automatic quantitative screening assay was developed using embryos from the *TG(Fli1:EGFP)* zebrafish line. The assay was implemented in a high-throughput screening platform (Biobide SL, San Sebastián, Spain) and includes automated methods for embryo dispensation, compound delivery, embryo imaging and processing of the results (details of automated methods are provided elsewhere, (Letamendia *et al*., submitted). Treated embryos were imaged and automatically analyzed for defects in ISVs development by measuring the fluorescence area in the embryo tail. A detailed analysis to quantify the effects on the total number of ISVs formed, as well as the number of complete ISVs formed (that is, the number of ISVs that reach the dorsal longitudinal anastomotic vessel uninterrupted), was carried out for the positive compounds. Following an initial screen of 288 compounds, seven compounds were identified that showed dose-dependent anti-angiogenic activity with low toxicity, giving a hit rate of just under 2.5%. The data obtained for compounds F10 and F11 is shown in Figure 1. For each compound, an image acquired at the concentration at which a statistically significant decrease in ISV formation is detected is shown (Figures 1a and d), and the decrease in total ISV formation (Figures 1b and e) and in the number of complete ISVs formed (Figures 1c and f) is plotted against the specific concentrations titrated. The data for the other 'hit' compounds is similarly provided in Supplementary Figures 2, 3 and 4.

The BioFocus SoftFocus library contains compounds that are selected as putative kinase inhibitors based on their structure. To elucidate the targets of the compounds isolated from our screen, *in-vitro* kinase profiling was performed on compounds that were identified as inhibitors of angiogenesis (Supplementary Figure 5). Kinase profiling identified PhK subunit G1 (PhKG1) as the kinase target of compound F11 (that is, showing less than 10% activity in the kinase profiling assay). Interestingly, PhKG1 was also inhibited by compound F10, albeit with weaker effect, among other kinases including TrKA and PIM1 (Supplementary Figure 5A). No kinase was inhibited to less than 10% activity by compound F10, indicating a less specific effect of this compound compared with F11. Careful titration of each compound under the kinase profiling conditions would allow a more accurate analysis of the difference in efficacy of each compound for PhKG1; however, the higher apparent toxicity level of F10, evident by comparing the overall appearance of the embryo at 10 μM F10 with 30 μM F11 (Figure 1), would support a more pleiotropic nature of this compound. These two compounds were taken forward for further studies and for validation of the kinase targets (the chemical structures of compounds F10 and F11 are shown in Supplementary Figure 5B).

To confirm that these two compounds inhibited specifically the angiogenic process of ISV sprouting, as opposed to inhibition of general vasculogenesis, embryos were treated at 10 hpf, before the vasculogenic vessels had formed. An overnight treatment with 5 μM of either drug at this time point lead to almost complete inhibition of ISV growth with no inhibitory effect on the DA, confirming that normal vasculogenic processes, by which the DA is formed, were not affected by either compound (Supplementary Figure 6A), despite the strong effect observed on ISV sprouting, which is an angiogenic process. In addition, treatment with the compounds at 3 days post fertilization (dpf) had no effect on the preexisting ISV (Supplementary Figure 6B), confirming that the compounds specifically inhibit the angiogenic process and do not target established blood vessels.

To study the effect of our compounds in a human cell-based *in vitro* test for angiogenesis, a basic assay of human umbilical vein endothelial cell (HUVEC) tube formation was performed (Figures 2a and b). A dose-dependent reduction in tube formation was observed in the presence of either compound, with an approximate IC_{50} of 6 μM for F10 and 20 μM for F11 (Figures 2a and b), indicating that both compounds have anti-angiogenic effect on human endothelial cells.

HUVEC cell migration was also assessed upon treatment with each compound using a transwell migration assay (BD Biosciences, Bedford, MA, USA). A dose-dependent reduction in the number of cells that migrated was observed in the presence of each compound ($IC_{50} = 1.5$ μM for both compounds; Figures 2c and d), indicating a strong inhibitory effect of both compounds on HUVEC cell migration.

Additionally, a cell proliferation assay was performed to assess the effect of each compound on HUVEC proliferation. A concentration range of 1–50 μM of each compound was tested and dose-dependent decrease in cell proliferation was observed in the presence of compound F10 above a concentration of 7 μM (Figure 2e). However, the proliferation rate never decreased to below 50% of the untreated activity and no effect on proliferation or viability is observed at either 1.5 μM (the IC_{50} of HUVEC cell migration inhibition) or 6 μM (the IC_{50} of HUVEC tube formation inhibition). No decrease in cell proliferation was observed in the presence of compound F11 (Figure 2e), indicating that this compound does not inhibit HUVEC proliferation or show toxicity over the

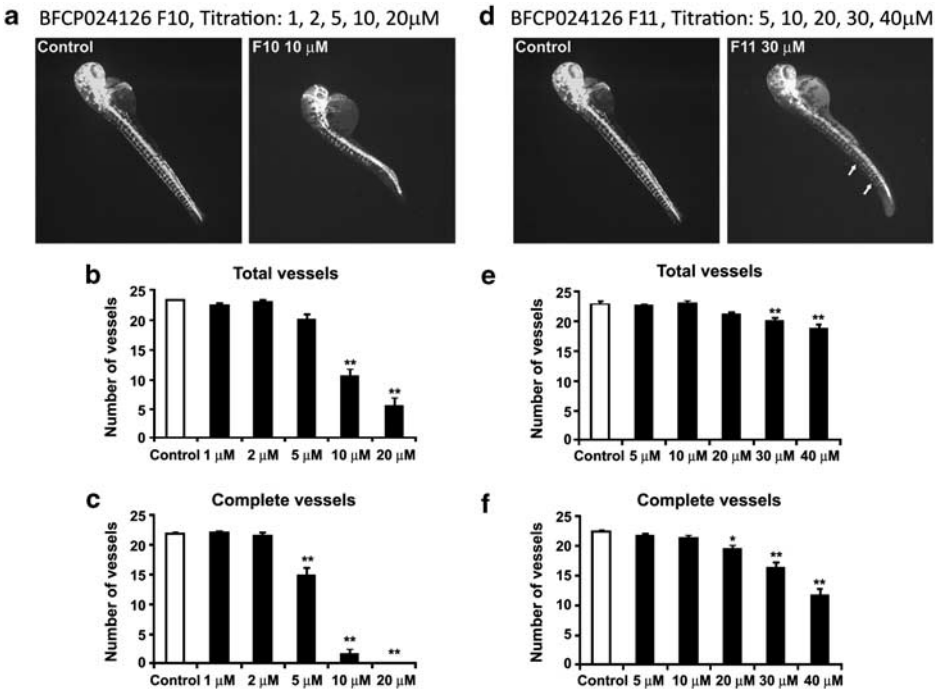

Figure 1 Dose-dependent effect of compounds on ISV formation. A titration of 1, 2, 5, 10 and 20 μM compound F10 (**a**–**c**) or 5, 10, 20, 30 and 40 μM compound F11 (**d**–**f**) was performed, as indicated. Images were acquired using the automated imaging acquisition system (**a**, **d**) and the effects of each compound on ISV total number (**b**, **e**) and on the number of complete ISVs formed (**c**, **f**) at each concentration tested were determined and depicted graphically. $*P \leqslant 0.05$. $**P \leqslant 0.01$.

concentration range tested. Therefore, the inhibition of tube formation and migration of HUVEC cells in the presence of either compound is not a result of decreased HUVEC proliferation or cell viability, indicating that the primary effect of the compounds is the suppression of endothelial cell function rather than cytotoxicity.

To further confirm the anti-angiogenic properties of the two compounds, we performed a longer-term assay for studying the formation of capillary-like structures, as described in Supplementary Materials and Methods. The HUVEC cells initially form small islands within the culture matrix, but enter a migratory phase, resulting in thread-like tubule structures upon proliferation. After 8–11 days, they form a branched network of anastomosing tubules in a process that more closely resembles physiological angiogenesis. Two days after the cells were seeded, they were treated with either compound F10 or F11, at the indicated concentrations (Figure 3). A dose-dependent reduction in tube formation was observed with both compounds following 11 days of treatment, and both compounds completely inhibited capillary formation at 5 μM.

Having identified PhKG1 as the kinase target of compound F11 and a potential target of compound F10, we wished to analyze the involvement of PhKG1 in the anti-angiogenic effects observed by treatment with these two compounds. To this end, we tested whether overexpression of PhKG1a (the ortholog of PhKG in zebrafish) could reduce the anti-angiogenic effect of the two compounds in zebrafish, an experiment that is analogous to situations in which a drug effect is overcome by increased gene copy number (Ferguson, 1991). Treatment with low concentrations (suboptimal for strong ISV inhibition so that neither compound was saturating) of either compound caused a mild inhibition of ISV formation over a 24-h treatment. Injection of PhKG1a mRNA lead to at least partial rescue of ISV inhibition (Figure 4, percentages of embryos showing partial and complete rescue are shown to the right), suggesting that the inhibition of PhK by compounds F10 and F11 is an important factor in the anti-angiogenic properties of both compounds and further highlighting the role of PhKG1 in angiogenesis.

To investigate the interaction between PhKG1 and compounds F10 and F11, we performed a three-dimensional modeling analysis of the interaction site. Space-filling models of BioFocus SoftFocus compounds F10 and F11 docked into the catalytic site of PhKG1 are shown in Supplementary Figure 7A and 7B, respectively. The western part of the compounds is completely planar and fits snugly in the especially tight hinge region of PhKG1. The aminomethylene linker positions the eastern parts of the compounds well for further interactions with the protein. Two-dimensional cartoons of the interactions that compound F10 (Supplementary Figure 7C) and F11 (Supplementary Figure 7D) make with the protein are also provided. Both compounds accept a hydrogen bond from the NH group of Met106. One or two aromatic C–H…O hydrogen bonds (not indicated) can also be formed. The aromatic rings of both compounds are positioned such that several interactions can be formed between the backbone NH groups and the π-clouds of these aromatic rings. Compound F11 accepts a hydrogen bond from the side

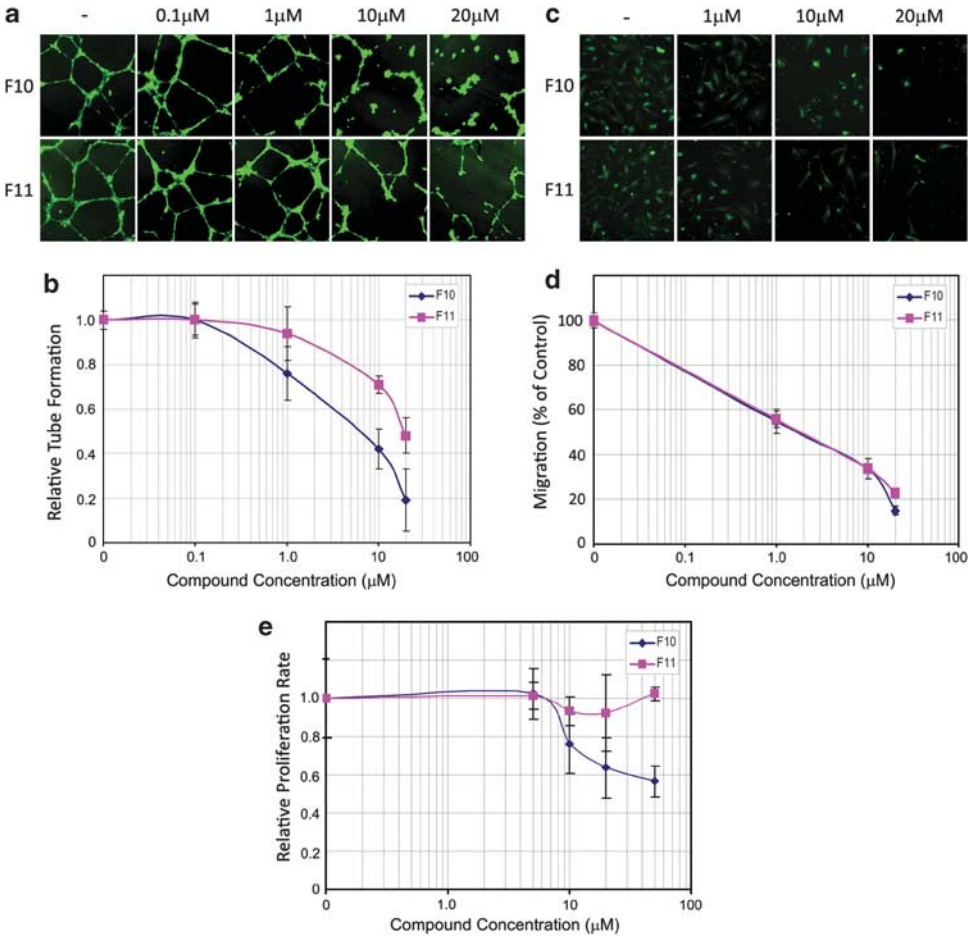

Figure 2 Compounds F10 and F11 show inhibitory effects in human *in-vitro* angiogenesis assays. (**a**) HUVEC cells were plated on matrigel in the absence or presence of 0.1, 1, 10 or 20 μM of either compound F10 or F11, as indicated. Tube formation was allowed to continue for 18 h, at which point cells were stained with Calcein AM and imaged. (**b**) Tubule lengths (from **a**) were measured from three fields of view from each well and the average length was plotted graphically against concentration of compound. (**c**) Serum-starved HUVEC cells were plated in the absence or presence of 1, 10 or 20 μM of either compound F10 or F11, as indicated, in the upper chamber of a transwell migration assay kit and allowed to migrate towards serum-supplemented medium in the lower chamber over a 20-h period. (**d**) Migrated cells (from **c**) were stained with Calcein AM and the number of migrated cells was counted in three fields of view from each well and the average number plotted against compound concentration. (**e**) HUVEC cells were seeded in a 96-well plate and treated with a titration of 5, 10, 20 or 50 μM of either compound F10 or F11, as indicated, for 20 h. A WST-1 proliferation assay was performed and the proliferation rate relative to the untreated control cells was plotted against compound concentration.

chain amine of Lys48, whereas F10 does not. F11 also makes a tighter interaction with the hinge region (around Met106) than F10. These two effects combined may explain why F11 is somewhat more active than F10. The activity of these compounds combined with a unique binding mode provides a good starting point for compound optimization and further drug discovery efforts.

To further analyze the role of PhKG in angiogenesis, we employed specific morpholino knock down of PhKG1a in the *TG(Fli1:EGFP)* zebrafish line. Injection of PhKG1a-specific morpholino demonstrated that knock down of this kinase had a particularly marked effect on angiogenesis, with inhibition of ISV growth observed in at least 97% of injected embryos, compared with mock injected controls. PhKG1a knock down led to incomplete formation of all ISV and the complete failure of dorsal longitudinal anastomotic vessel formation (Figure 5, upper panel). To confirm the specificity of the phenotype observed, phenotypic rescue experiments were performed by co-injection of PhKG1a mRNA. Rescue by concurrent injection of PhKG1a mRNA was observed in over 80% of injected embryos (Figure 5, lower panels). No effect of PhKG1a mRNA alone was observed. This data strongly implicates a function of PhKG1a in the angiogenic process. This is the first report of PhKG1 being implicated in angiogenesis, identifying a novel potential target for the treatment of cancer by angiogenesis inhibition. No effect on ISV formation was observed in the presence of a mismatch control morpholino (in which five bases are substituted; Figure 5, labeled Ctrl), further confirming the specificity of the effects observed.

Previous reports concerning PhK focus on its role during metabolism and concentrate on its expression in the liver. To determine if PhKG1a is expressed in zebrafish embryos during angiogenesis, we performed *in situ* hybridization with a PhKG1a-specific probe on

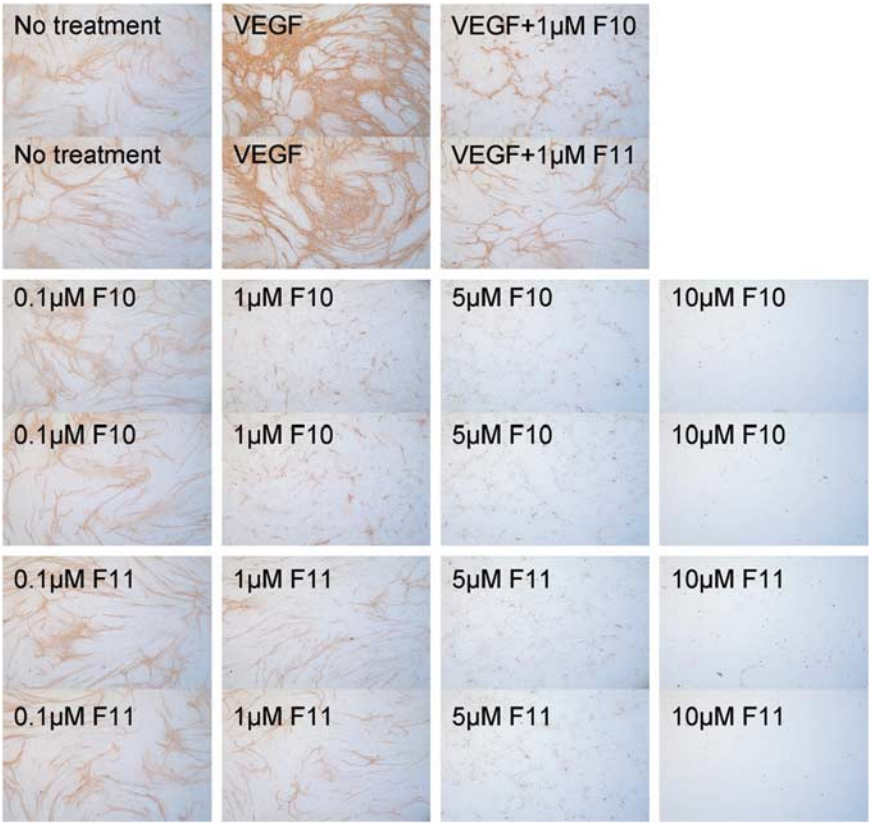

Figure 3 Compounds F10 and F11 inhibit HUVEC capillary growth. A long-term HUVEC capillary-like tubule formation assay was performed, in which HUVEC cells were plated over a matrix of human fibroblasts and allowed to form tubules over a period of 11 days in the presence of 0.1, 1, 5 or 5 μM of compound F10 (middle panels) or F11 (lower panels), as indicated. Duplicate experiments are shown. Tube formation upon treatment is compared with a non-treatment control, 2 ng/ml VEGF angiogenesis stimulant and 2 ng/ml VEGF in the presence of 1 μM of either compound F10 or F11 (upper panels, as indicated).

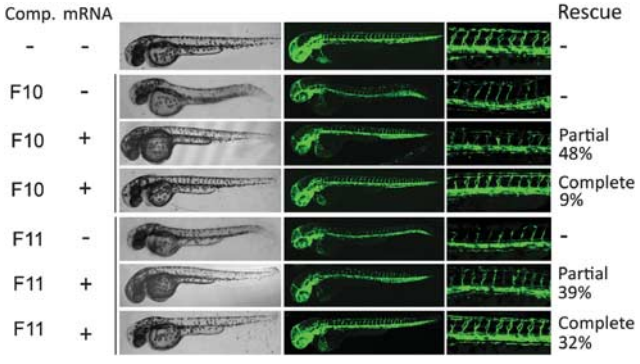

Figure 4 A component of the anti-angiogenic effect of the compounds is PhKG1-dependent. Single-cell stage embryos were mock-injected or injected PhKG1a mRNA (as indicated in the first column to the left of the panels) and then treated at 24 hpf with either 3 μM of compound F10 or 5 μM of compound F11, as indicated. The rescue of ISV formation from a 24 h treatment with compound F10 by injection of PhKG1a mRNA is shown in the upper panels. The rescue of ISV formation from treatment with compound F11 by injection of PhKG1a mRNA is shown in the lower panels. The number of embryos showing either partial or complete rescue of ISV formation is shown as a percentage to the right of the panels.

TG(Fli1:EGFP) zebrafish embryos at 24, 36 and 48 hpf (Supplementary Figure 8). A strong PhKG1a-specific signal was observed along the DA (from which the ISVs sprout) at the 24 hpf stage (Supplementary Figure 8A). The signal was weaker at 36 hpf and undetectable by 48 hpf, indicating that PhKG1a mRNA levels are elevated during early stages of embryogenesis, but that by 48 h PhKG1a mRNA is no longer strongly expressed. No PhKG1a was detected in the ISVs themselves, suggesting that sprouting of ISVs from the DA is dependent upon, or driven by, PhKG1a expression in the dorsal vasculature. The timing of expression supports this, as ISV sprouting begins at 16–19 hpf and by 36–40 hpf the ISVs are fully formed and would therefore not require further expression of angiogenic signals. The signal specificity is confirmed by hybridization using the sense probe control (Supplementary Figure 8B). A GFP control is included to clarify the vasculature structures and the timing of ISV sprouting and growth (Supplementary Figure 8C). Incidentally, early expression of PhKG1a would coincide with the timing of morpholino activity and expression. Furthermore, the timing of PhKG1a mRNA expression is

consistent with the effectiveness of F10 and F11 activity during treatment of early stage embryos (Figure 1 and Supplementary Figure 6A) and their lack of activity when used to treat 3 dpf embryos (Supplementary Figure 6B).

To validate the role PhKG1 human cell-based angiogenesis assays, we performed tube formation, cell migration and proliferation assays in HUVEC cells in which PhKG1 was specifically knocked down by siRNA targeting (Figure 6). A 50% reduction in tube formation was observed in the presence of PhKG1-specific siRNA compared with the control siRNA (Figure 6a). PhKG1 knockdown caused an even more striking reduction in cell migration, with five-fold fewer cells migrating in the presence of PhKG1-specific siRNA compared with control siRNA (Figure 6b). No reduction in cell proliferation was observed (Figure 6c), confirming that the effects were specific and not caused by general toxicity or reduced proliferation. The level of PhKG1 knockdown is shown in Figure 6d. The identification and validation of the compounds' target represents an important advancement on previous screens (in which compounds are often identified that have a strong effect on the desired screening parameter, but the mode of action is rarely elucidated), as it enables rational optimization of the compounds identified to increase their efficiency and specificity towards the target.

There are no previous reports of PhK involvement in cancer progression or angiogenesis. We were therefore interested to determine if there is a link between PhKG1 function and cancer. We therefore searched The Cancer Genome Atlas (TCGA) data (website retrieved through the CGWB website), which integrates publicly available cancer data from various projects, and compiled data of *PhKG1* gene copy number in tumor samples (https://cgwb.nci.nih.gov/). Interestingly, amplification of *PhKG1* occurs in a high number of TCGA tumor samples tested (between 22–75%, depending on the tumor type; Table 1). PhK is a complex holoenzyme consisting of four different types of subunit, α, β, γ and δ.

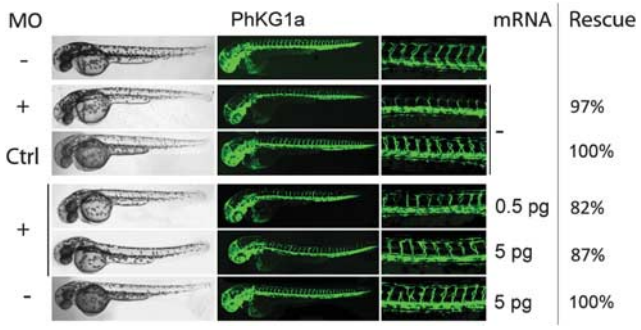

Figure 5 PhKG1a knockdown in zebrafish inhibits angiogenic ISV formation. Single-cell stage embryos were injected with 0.2 of PhKG1a-specific morpholino or 0.2 μM of a control morpholino, in which five bases are substituted, as indicated (upper panels). The effects on ISV formation were assessed manually. The specificity of the PhKG1a morpholino was confirmed by co-injection of 0.5 or 5 pg of PhKG1a mRNA (lower panels), which leads to dose-dependent rescue of ISV formation. Injection of 5 pg of PhKG1a mRNA alone had no effect (bottom panel). Percentages of injected embryos showing phenotype and phenotypic rescue are shown to the right of the panels.

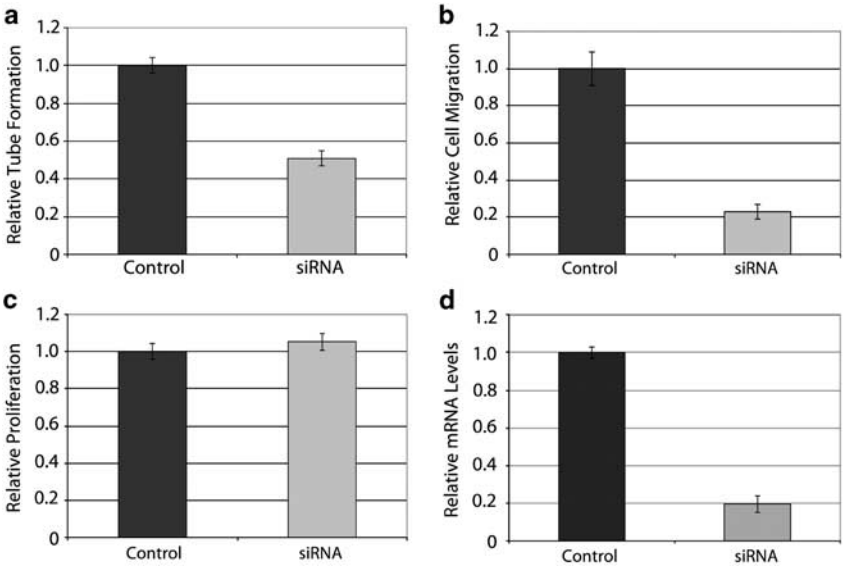

Figure 6 PhKG1 knockdown reduces HUVEC tube formation and migration. (**a**) HUVEC cells were transfected with PhKG1 targeting siRNA or control siRNA, as indicated, and tube formation assays were performed, measured and plotted as in Figure 2. (**b**) Serum-starved HUVEC cells, transfected with either PhKG1 targeting siRNA or control siRNA, as indicated, were plated in a transwell migration assay kit and assayed, counted and plotted as in Figure 2. (**c**) HUVEC cells, transfected with either PhKG1 targeting siRNA or control siRNA, as indicated, were seeded in a 96-well plate. aWST-1 proliferation assay was performed as in Figure 2. (**d**) RNA was extracted from HUVEC cell pellets taken at the time of seeding the above assays, and Q–PCR was performed using two sets of PhKG1-specific probes to determine level of PhKG1 knockdown (plotted as the relative level of PhKG1 mRNA in each sample).

Table 1 Aberrations in gene copy number of PhK subunits in tumor samples

	PhKG1 amplification (%)	*PhKA deletion (%)*	*Either (%)*
GBM	201/267 (75)	140/210 (67)	91
LUSC	29/59 (49)	50/59 (85)	97
LUAD	7/21 (33)	12/21 (57)	67
COAD	37/77 (48)	44/77 (57)	78
BRCA	28/92 (30)	43/92 (47)	58
Ovarian serous cystadenocarcinoma	80/368 (22)	190/268 (52)	59
READ	17/34 (50)	15/34 (44)	74

Abbreviations: BCRA, breast invasive carcinoma; COAD, colon adenocarcinoma; GBM, glioblastoma multiform; LUAD, lung adenocarcinoma; LUSC, lung squamous cell carcinoma; PhK, phosphorylase kinase; PhKG1, PhK subunit G1; READ, rectal adenocarcinoma.
Data from The Cancer Genome Atlas (TCGA) datasets on the Cancer Genome Work Bench (CGWB) website.
The number of tumor samples that show either amplification in PhKG1 gene copy number (PhKG1 amplification) or reductions in PhKA copy number (PhKA deletion) is shown by tumor sample type (indicated in the first column). Data is expressed as the number of samples showing the relevant aberration out of the total number of samples analyzed, along with the same information expressed as a percentage. The final column shows the number of individual tumor samples that show either one of the two events (PhKG1 amplification or PhKA deletion), expressed as a percentage of the total number of tumor samples.

PhKG1 (the γ-subunit) is the catalytic subunit and upregulation of this subunit would lead to increased-PhK activity. The α- and β-subunits are inhibitory subunits that restrain the enzymatic activity. Downregulation of these subunits would thus also be expected to lead to increased PhK activity. We therefore analyzed if downregulation of PhK subunit-α (the largest of the regulatory subunits) is a common feature of the TCGA tumor samples analyzed and discovered that *PhKα* deletion (decreased copy number) is very common, with between 44–85% of tumor samples showing PhKα deletion (Table 1). We then analyzed the correlation between *PhKG1* amplification and *PhKα* deletion within individual tumors, determining the number of tumors that showed an anomaly in either subunit that would be expected to lead to increased-PhK activity (that is, either *PhKG1* amplification or *PhKα* deletion). The total number of tumors that show an aberration in at least one of these subunits of the PhK holoenzyme is extremely high, ranging from 59% in ovarian serous cystadenocarcinoma to 97% of lung squamous cell carcinoma samples showing either an amplification of *PhKG1* or deletion of *PhKα*, indicating that there is a strong link between PhK aberration and tumorigenesis. This highlights the relevance of PhK as a potential therapeutic target.

Having identified PhK as a kinase that shows a high incidence of gene copy number aberrations by TCGA copy number variation profiling, we were interested to establish a concrete correlation between copy number and mRNA levels. We therefore examined the incidence of gene copy number aberrations in commercially available cell lines, with which we could easily determine PhKG1 mRNA levels by quantitative PCR. Approximately 65% (135/207) of tumor cell lines tested in the GlaxoSmithkline Cancer Cell Line Genomic Profiling Data on the CGWB website (https://cgwb.nci.nih.gov/) showed an amplification of the mean copy number of the *PhKG1* gene (Table 2). To determine if this amplification translates into an increase in mRNA expression level, we chose five colon cancer cell lines, which represent a cancer type that has been approved for clinical trials of angiogenesis inhibitors, and performed quantitative PCR for PhKG1 levels. Two of the cell lines included, LS174T and Colo320 were shown by the GlaxoSmithkline analysis to have normal *PhKG1* copy number, whereas SW620, Colo201 and NCIH747 were all shown to have some degree of PhKG1 copy number amplification. By quantitative PCR, we found a correlation between the published gene copy number and mRNA levels in four out of five of the cell lines tested, and that two cell lines, Colo201 and NCIH747, do indeed express high levels of PhKG1 mRNA compared with human fibroblast control or cancer cells with normal copy number of PhKG1 (approximately

Table 2 Amplifications of PhKG1 gene copy number in tumor cell lines

	PhKG1 amplification	*Total*	*%*
Bladder	8	10	80
Brain	3	7	43
Breast	16	21	76
CNS	7	11	64
Cervix	4	7	57
Colon	11	19	58
Kidney	5	8	63
Liver	5	9	56
Lung	54	79	68
Muscle	2	4	50
Ovary	5	7	71
Rectum	2	2	100
Sarcoma	1	2	50
Stomach	3	5	60
Thyroid	3	4	75
Uterus	4	9	44
Vulva	2	3	67
Total	135	207	65

Abbreviation: CGWB, Cancer Genome Work Bench; CNS, central nervous system; GSK, GlaxoSmithkline; PhKG1, phosphorylase kinase subunit G1.
Data from GSK Cancer Cell Line Genomic Profiling Data on the CGWB website.
The number of cancer cell lines that show amplifications in the PhKG1 (PhKG1 amplification) gene copy number out of the total number of cell lines analyzed (Total) is shown. The final column expresses the same information as a percentage (the percentage of tumors that show PhKG1 amplification out of the total number analyzed). The data is shown for each individual cell line type (indicated in the first column), as well as across all of the cell lines combined (final row).

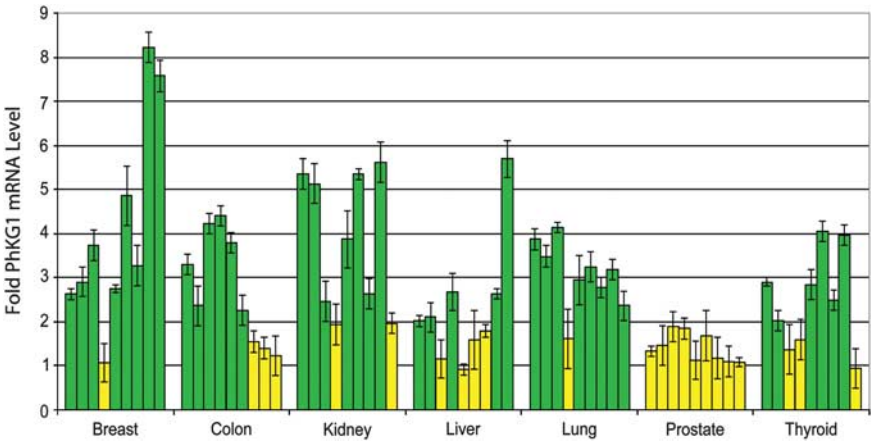

Figure 7 PhKG1 is upregulated in human tumor samples from a range of tumor types. Q–PCR was performed using PhKG1-specific probes on duplicate TissueScan Cancer Survey cDNA arrays. Green bars indicate samples in which the PhKG1 mRNA level is more than two-fold the average PhKG1 level present in the tissue-matched normal tissue controls. Yellow bars indicate no change (that is, less than two-fold difference compared with the average PhKG1 level in the tissue-matched controls).

five times and three times the control levels, respectively; Supplementary Figure 9). This data suggests that amplification of *PhKG1* copy number does lead to an increase in PhKG1 mRNA expression levels in these lines.

Furthermore, we examined the relative PhKG1 levels in a panel of different human tumor samples, obtained as a commercially available cDNA array. Using quantitative PCR, we discovered that PhKG1 mRNA levels are elevated by more than two-fold (green bars) in the majority of human tumors tested (Figure 7). Interestingly, there was no upregulation of PhKG1 detected in prostate cancer, suggesting that PhKG1 upregulation, although common, is not a universal characteristic of all tumor types and that prostate cancer may not represent a type that would benefit from PhKG1 targeting. This data provides the first evidence of upregulated PhKG1 mRNA expression levels in a variety of human tumor types and suggests that an upregulation of PhKG1 could be associated with cancer progression.

Discussion

PhKG1 has not previously been implicated in either tumorigenesis or angiogenesis. We therefore provide here the first description of the involvement of PhK in the angiogenesis process and the first identification of PhK as a novel therapeutic target. Rescue of the phenotype observed under subsaturating concentrations of either compound by overexpression PhKG1 (through injection of mRNA) confirms that a component of the anti-angiogeneic effect of both compounds is dependent on inhibition of PhKG1. This rescue is analogous to drug resistance conferred by gene copy number amplification, such as clinical resistance to STI-571 due to amplifications in *bcr-abl* gene copy number (Gorre *et al*., 2001) and resistance to methotrexate in acute leukemia due to *dihydrofolate reductase* amplification (Carman *et al*., 1984; Goker *et al*., 1995) among others (Ferguson, 1991). The level of rescue obtained in the presence of F10 was substantially lower than that observed in the presence of F11, which is likely to reflect the stronger inhibitory effect of compound F11 on PhKG1 and the more pleiotropic nature of compound F10 (from the profiling data). This pleiotropicity could also explain the increased toxicity observed in both the zebrafish whole organism models and the HUVEC WST-1 assay in the presence of compound F10. Few embryos showed complete rescue by PhKG1 overexpression (particularly in the case of F10), suggesting that there could be other kinases affected by the compounds, in keeping with the fact that these are early stage compounds that have not undergone any form of optimization. Other kinases that showed weak inhibition during the kinase profiling include TrKA and PIM1; inhibition of these additional kinases by F10 and F11 could therefore explain the incomplete phenotypic rescue observed upon overexpression of PhKG1 mRNA.

PhK is an $(\alpha\beta\gamma\delta)_4$ holoenzyme that regulates glycogenolysis through phosphorylation, and thereby activation, of glycogen phosphorylase, which releases glucose 1-phosphate from glycogen, feeding into the glycolysis pathway to allow production of ATP. Glycogen phosphorylase is a fundamental enzyme in glycogen metabolism and PhK is the only enzyme known to catalyze its activation (Graves *et al*., 1999). The link between metabolism and tumor progression currently represents an exciting direction in cancer research, as the importance of metabolic transformation for maintaining the tumorigenic state becomes clearer (for reviews, see Kroemer and Pouyssegur, 2008; Tennant *et al*., 2010). Interestingly, the inhibition of key enzymes involved in glycogen metabolism has been shown to have a great effect on the angiogenic potential of HUVEC cells (Vizan *et al*., 2009), indicating that inhibition of metabolic pathways could offer novel therapeutic approaches that target both the angiogenesis pathway, as well as inhibit the actual growth and maintenance of tumor cells themselves. Metabolic pathways are therefore becoming an increasingly popular area of research into novel pathways for therapeutic intervention

(Cascante *et al*., 2010). We show that PhKG1 is upregulated in human tumors, identifying a previously unknown link between PhK and cancer. In fact, the percentage of tumors showing either loss of PhKα or gain of PhKG1 is strikingly high, with almost all of the lung squamous cell carcinoma samples analyzed showing a relevant aberration in at least one of the two subunits. Whether there is a direct correlation between the role of PhK in metabolism and cancer remains to be studied. However, we have demonstrated a clear role of PhKG1 in angiogenesis and migration of endothelial cells, which indicates that PhK could have a role in the angiogenic switch that leads to tumor vascularization, which is likely to link its function to tumor progression. The potential involvement of PhK in both aspects of tumor progression (angiogenesis and tumor metabolism) makes it an attractive target candidate for clinical intervention.

Recently, there has been a shift towards 'rational' drug design, in which a drug is designed to target a specific protein or pathway known to be involved in tumorigenesis (Lane *et al*., 2010). However, screening libraries vastly increases the number of candidate compounds to be discovered and in many ways is a much simpler and more cost effective approach. In light of the fact that we identify and validate the targets of our compounds, our results highlight the advances in technology that make high-throughput screening a valuable source of compound discovery and emphasize the value of zebrafish as a model organism that lends itself to high-throughput screening techniques, whilst providing very relevant screening parameters due to the whole-organism setting.

Here we identify kinase-inhibitor compounds that cause marked inhibition of angiogenesis in both zebrafish whole organisms and in human *in vitro* cell-based angiogenesis assays. Furthermore, we determine the kinase target, offering an important advancement on many previous screens in which the compound targets are not elucidated, and identify a previously undiscovered role of PhKG1 in angiogenesis. Our results provide the first evidence of the PhK holoenzyme having a role in tumorigenesis, offer further insight into the process of angiogenesis and establish PhKG1 as a novel anti-angiogenic therapeutic target.

Materials and methods

Zebrafish husbandry and compound screening
Adult *TG(Fli1:EGFP)* zebrafish were housed and maintained in accordance with standard procedures. Screening was performed in an automatic HTS platform (Biobide), as described in Supplementary Materials and Methods. Kinase profiling was performed in The National Centre for Protein Kinase Profiling at the MRC Protein Phosphorylation Unit (Dundee, UK), and kinases that show less than 10% activity in the screen are considered to be compound targets.

Morpholino experiments
Specific morpholino against PhKG1a and the control morpholino (GeneTools LLC, Philomath, OR, USA) were reconstituted in RNAse-free water according to manufacturer's instructions. Volumes of 0.1–1 μM were titrated into single-cell embryos ($n = > 100$) and the lowest effective dose (0.2 μM) was used for all experiments. Zebrafish *PhKG1a* gene was cloned into pGEM-T vector using the pGEM-T easy Vector system I (Promega BioSciences, LLC. San Luis Obispo, CA, USA) according to manufacturer's instructions, and mRNA was synthesized using mMessage Machine (Ambion, Life Technologies, Grand Island, NY, USA). For the rescue of F10 and F11 phenotype by PhKG1a mRNA, embryos were injected at the single-cell stage with a titration of PhKG1 mRNA and treated with 3 μM of F10 or 5 μM of F11 at 24 hpf for 24 h. Rescue with 10 pg of PhKG1a mRNA for compound F10 and 20 pg mRNA for compound F11 is shown.

In situ hybridization was performed as described in (Pownall *et al*., 1996). Sense and anti-sense probes were synthesized using the pGEMT PhKG1a plasmid template using mMessage Machine (Ambion).

HUVEC assays
HUVEC cells were obtained from BD Biosciences and maintained at 37 °C with 5% CO_2 in endothelial cell culture medium (BD Biosciences). The basic tube formation assay was performed in a 96-well plate coated with ECMatrix (Millipore, Billerica, MA, USA), as previously described (Tran *et al*., 2007). Cells were treated in triplicate with compound F10 or F11 (or dimethyl sulfoxide control), as indicated. Tubes were stained with fluorescent dye Calcein AM (Invitrogen, SA, Life Technologies, Grand Island, NY, USA) and imaged with a Leica fluorescence microscope (Leica Microsystems, Milton Keynes, UK).. The length of tubule extensions from cell bodies was measured using LAS AF software (Leica Microsystems) and the average total length from three fields of view per well was determined.

The HUVEC migration assay was performed using the transwell biocoat endothelial cell migration angiogenesis system (BD Biosciences), according to manufacturer's instructions. Cells were seeded into the upper chamber in the presence of a titration of F10 or F11 (or dimethyl sulfoxide control) in triplicate and endothelial growth medium containing 10% fetal calf serum was placed in the lower chamber as a chemoattractant. Calcein AM was added to the lower chamber and cells were imaged using a Leica fluorescence microscope. The number of migrated cells were counted and shown as an average of three fields per well.

A WST-1 Cell proliferation Assay (Roche Applied Science, Roche Diagnostics Ltd, Burgess Hill, UK) was performed according to manufacturer's instructions. Cells were seeded in a 96-well plate and treated with F10 or F11, in triplicate, as indicated. After 20 h of treatment, the WST-1 reagent was added. Absorbance was read at 450 nm on a BioTek PowerWave XS (BioTek Germany, Bad Friedrichshall, Germany) microtitre plate reader.

siGENOME SMARTpool siRNA against PhKG1 and control siRNA (Thermo Fisher Scientific, Dharmacon Products, Lafayette, CA, USA) were transfected according to the Dharmcon HUVEC transfection protocol, using DharmaFECT transfection reagent 4.

Quantitative PCR
Total RNA was isolated from cell lines using Trizol (Invitrogen), followed by cDNA synthesis using Superscript II Reverse Transcriptase (Invitrogen). Quantitative PCR was performed on cDNA from cell lines using SYBR GREEN PCR Master Mix (Applied Biosystems, Life Technologies, Grand Island, NY, USA). Results were validated using two independent primer sets for human PhKG1. Q–PCR on duplicate

TissueScan Cancer Survey cDNA Array 96-1 (OriGene, Rockville, MD, USA) were performed according to manufacturer's instructions using SYBR GREEN, as above.

Conflict of interest

The authors declare no conflict of interest.

Acknowledgements

We would like to thank Cornel Catana of Galapagos for molecular modeling efforts and acknowledge the support and intellectual contribution of the Scientific Director of Biobide, Carles Callol. This project was financially supported by the European Community under the FP7 ZF-Cancer project (HEALTH-F2-2008-201439), MICINN and Fundacion Cellex.

References

Berghmans S, Murphey RD, Wienholds E, Neuberg D, Kutok JL, Fletcher CD *et al*. (2005). tp53 mutant zebrafish develop malignant peripheral nerve sheath tumors. *Proc Natl Acad Sci USA* **102**: 407–412.

Carman MD, Schornagel JH, Rivest RS, Srimatkandada S, Portlock CS, Duffy T *et al*. (1984). Resistance to methotrexate due to gene amplification in a patient with acute leukemia. *J Clin Oncol* **2**: 16–20.

Carmeliet P, Jain RK. (2000). Angiogenesis in cancer and other diseases. *Nature* **407**: 249–257.

Cascante M, Benito A, Zanuy M, Vizan P, Marin S, de Atauri P. (2010). Metabolic network adaptations in cancer as targets for novel therapies. *Biochem Soc Trans* **38**: 1302–1306.

Edmunds SC, Kelsell DP, Hungerford JL, Cree IA. (2002). Mutational analysis of selected genes in the TGFbeta, Wnt, pRb, and p53 pathways in primary uveal melanoma. *Invest Ophthal Vis Sci* **43**: 2845–2851.

Eilken HM, Adams RH. (2010). Dynamics of endothelial cell behavior in sprouting angiogenesis. *Curr opin cell biol* **22**: 617–625.

Faucherre A, Taylor GS, Overvoorde J, Dixon JE, Hertog J. (2008). Zebrafish pten genes have overlapping and non-redundant functions in tumorigenesis and embryonic development. *Oncogene* **27**: 1079–1086.

Ferguson PJ. (1991). The role of gene amplification in clinical resistance to chemotherapy: a review. *J Otolaryngol* **20**: 130–136.

Folkman J. (2007). Angiogenesis: an organizing principle for drug discovery? *Nat Rev* **6**: 273–286.

Goker E, Waltham M, Kheradpour A, Trippett T, Mazumdar M, Elisseyeff Y *et al*. (1995). Amplification of the dihydrofolate reductase gene is a mechanism of acquired resistance to methotrexate in patients with acute lymphoblastic leukemia and is correlated with p53 gene mutations. *Blood* **86**: 677–684.

Gorre ME, Mohammed M, Ellwood K, Hsu N, Paquette R, Rao PN *et al*. (2001). Clinical resistance to STI-571 cancer therapy caused by BCR-ABL gene mutation or amplification. *Science* **293**: 876–880.

Gragoudas ES, Adamis AP, Cunningham Jr ET, Feinsod M, Guyer DR. (2004). Pegaptanib for neovascular age-related macular degeneration. *New Engl J Med* **351**: 2805–2816.

Graves D, Bartleson C, Biorn A, Pete M. (1999). Substrate and inhibitor recognition of protein kinases: what is known about the catalytic subunit of phosphorylase kinase? *Pharmacol Ther* **82**: 143–155.

Hurwitz H, Fehrenbacher L, Novotny W, Cartwright T, Hainsworth J, Heim W *et al*. (2004). Bevacizumab plus irinotecan, fluorouracil, and leucovorin for metastatic colorectal cancer. *New Engl J Med* **350**: 2335–2342.

Isogai S, Horiguchi M, Weinstein BM. (2001). The vascular anatomy of the developing zebrafish: an atlas of embryonic and early larval development. *Dev Biol* **230**: 278–301.

Kidd KR, Weinstein BM. (2003). Fishing for novel angiogenic therapies. *Brit J Pharmacol* **140**: 585–594.

Kroemer G, Pouyssegur J. (2008). Tumor cell metabolism: cancer's Achilles' heel. *Cancer Cell* **13**: 472–482.

Lane DP, Cheok CF, Lain S. (2010). p53-based cancer therapy. *Cold Spring Harb Perspect Biol* **2**: a001222.

Lawson ND, Weinstein BM. (2002). *In vivo* imaging of embryonic vascular development using transgenic zebrafish. *Dev Biol* **248**: 307–318.

Letamendia A, Quevedo C, Ibarbia I, Virto JM, Holgado O, Diez M *et al*. Development and validation of an automated high-throughput system for zebrafish *in vivo* screenings. *Plos One* (submitted).

Liang D, Chang JR, Chin AJ, Smith A, Kelly C, Weinberg ES *et al*. (2001). The role of vascular endothelial growth factor (VEGF) in vasculogenesis, angiogenesis, and hematopoiesis in zebrafish development. *Mech Dev* **108**: 29–43.

Lyons MS, Bell B, Stainier D, Peters KG. (1998). Isolation of the zebrafish homologues for the tie-1 and tie-2 endothelium-specific receptor tyrosine kinases. *Dev Dyn* **212**: 133–140.

Marshall KE, Tomasini AJ, Makky K, Kumar SN, Mayer AN. (2011). Dynamic Lkb1-TORC1 signaling as a possible mechanism for regulating the endoderm-intestine transition. *Dev Dyn* **239**: 3000–3012.

Parng C, Seng WL, Semino C, McGrath P. (2002). Zebrafish: a preclinical model for drug screening. *Assay Drug Dev Technol* **1**: 41–48.

Pownall ME, Tucker AS, Slack JM, Isaacs HV. (1996). eFGF, Xcad3 and Hox genes form a molecular pathway that establishes the anteroposterior axis in Xenopus. *Development* **122**: 3881–3892.

Tennant DA, Duran RV, Gottlieb E. (2010). Targeting metabolic transformation for cancer therapy. *Nat Rev Cancer* **10**: 267–277.

Tran TC, Sneed B, Haider J, Blavo D, White A, Aiyejorun T *et al*. (2007). Automated, quantitative screening assay for anti-angiogenic compounds using transgenic zebrafish. *Cancer Res* **67**: 11386–11392.

Vizan P, Sanchez-Tena S, Alcarraz-Vizan G, Soler M, Messeguer R, Pujol MD *et al*. (2009). Characterization of the metabolic changes underlying growth factor angiogenic activation: identification of new potential therapeutic targets. *Carcinogenesis* **30**: 946–952.

Wang C, Tao W, Wang Y, Bikow J, Lu B, Keating A *et al*. (2010). Rosuvastatin, identified from a zebrafish chemical genetic screen for antiangiogenic compounds, suppresses the growth of prostate cancer. *Eur Urol* **58**: 418–426.

Supplementary Information accompanies the paper on the Oncogene website (http://www.nature.com/onc)